ICAS 2016
30th Congress of the International Council of the Aeronautical Sciences
DCC, Daejeon, Korea : September 25-30, 2016

AERODYNAMIC ANALYSIS WITH SEPARATION DYNAMICS OF A LAUNCHER AT STAGING CONDITIONS

Antonio Viviani*, Giuseppe Pezzella and Egidio D'Amato***
*** SUN, Second University of Naples, via Roma, Aversa. Italy,**
**** CIRA, Italian Aerospace Research Centre, via Maiorise, Capua. Italy**

Abstract

This paper deals with launcher aerodynamic design activities at phase-A level. The goal is to address the preliminary aerodynamic database of a next generation launch vehicle as input for performances evaluations as well as launcher control, sizing, and staging.
In this framework, different design approaches are considered. Indeed, steady computational fluid dynamics (CFD), with both Euler and Navier-Stokes approximations, are carried out to assess launcher aerodynamics. On the other hand, a coupled approach between unsteady CFD and a six degree-of-freedom trajectory analysis are exploited to address booster separation dynamics at staging conditions.

1 Introduction

During the development phase the launchers' needs for aerodynamic characterization are fulfilled by a hybrid approach encompassing wind tunnel testing (WTT) and computational fluid dynamics (CFD) results [1], [2], [3].

The joint use of WTT and CFD is a powerful tool, able to provide high quality data as input for performances evaluations as well as launcher control, sizing, and staging dynamics.

Aerodynamics for launcher systems focuses on the assessment of the loads the atmosphere determines over the quick moving and accelerating vehicle. These forces are applied through pressure and friction effects on the launcher surface, thus resulting in a global aerodynamic force [2], [3]. Therefore, the assessment of launcher aerodynamics is fundamental for the determination of the launcher's performances and control software. Indeed, in the motion direction, the aerodynamic drag slows the launcher.

On the other hand, the global aerodynamic force generally does not act at vehicle centre of gravity (CoG) location, then the aerodynamic moment exerted at the CoG can lead to stable or unstable behavior of the launcher, to account for in the launcher's control software [4].

Moreover, launchers structures and protrusions should sustain the aerothermal loads (i.e. local pressure and convective heat flux overshoots) all along the ascent trajectory. This also should be taken into account in the general loading studies devoted to the launcher sizing and thermal protection [5],[6].

Separation dynamics analysis at staging conditions is another design issue to address [7].

In this framework, the present research effort describes typical analyses carried out at Phase-A design level. Indeed, fully three-dimensional steady and unsteady computational fluid dynamics (CFD) analyses have been extensively addressed to feed launcher aerothermal design. The range between Mach 0.5 and 5 was investigated to assess the flowfield past the launcher during all critical flying phases. In particular, the analysis of stage separation dynamics is undertaken by fully coupling unsteady CFD simulation with six degree of freedom (6 dof) trajectory simulation of the exhaust booster stage. To this end, dynamic meshing approach has been exploited within unsteady CFD analysis.

Finally, note that numerical flowfield analysis and 6 dof trajectory simulations are performed with Fluent code and perfect gas flow model.

2 Launcher Configuration

The launcher vehicle features a hummer head cylinder, as main body, with two boosters, see Fig. 1. Non-dimensional aeroshape sizes are

also reported in figure, being launcher height L the reference length. As shown, the aeroshape under investigation also features a central core stage with a remarkable boat-tail configuration, which ends in correspondence of booster stage. The fairing diameter is 16% launcher height, while that of booster is equal to 0.076L. Booster is forty percent of whole launcher's height [8].

Finally, it is worth noting that this launcher configuration is close to that expected for ARIANE VI concept, being developed by European Space Agency (ESA).

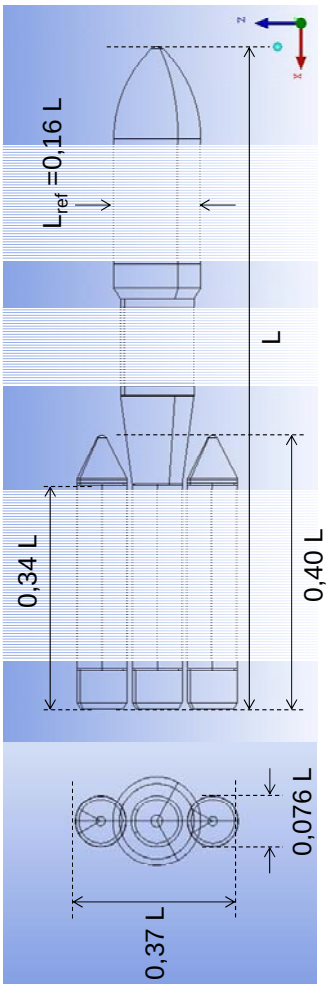

Fig. 1. The Launcher configuration.

3 Flowfield Analysis and Longitudinal Aerodynamic Appraisal

Aerodynamic data for launchers are provided in the body reference frame (BRF) as illustrated in Fig. 2 [2], [3], [4]. In this figure, aerodynamic force and moment coefficients are also provided, with sign convention according to the ISO norm. 1151[2].

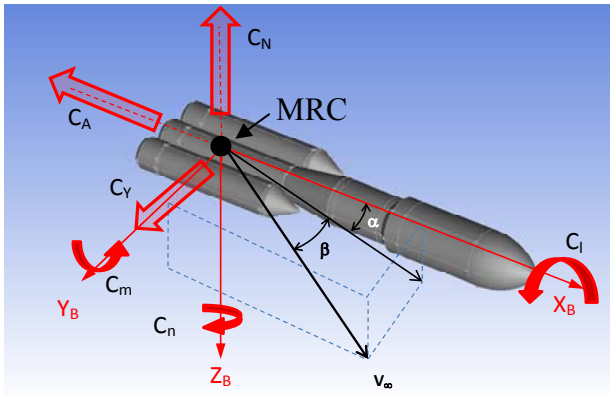

Fig. 2. Body reference frame with aerodynamic sign convention according to ISO 1151.

The global aerodynamic force $\vec{F}$ and moment $\vec{M}$ acting on the launcher are expressed in BRF as follows:

$$\vec{F} = S_{ref} q_\infty \left(-C_A \hat{i} + C_Y \hat{j} - C_N \hat{k} \right) \qquad (1)$$

$$\vec{M} = S_{ref} L_{ref} q_\infty \left(C_l \hat{i} + C_m \hat{j} + C_n \hat{k} \right) \qquad (2)$$

where C_A: axial force coefficient, C_Y: transverse force coefficient, C_N: normal force coefficient, C_l=C_{Mx}: rolling moment coefficient, C_m=C_{My}: pitching moment coefficient, C_n=C_{Mz}: yawing moment coefficient, $\left(\hat{i}, \hat{j}, \hat{k}\right)$ are the reference unit vectors, S_{ref}: reference surface, L_{ref}: reference length (see Fig. 1), q_∞: dynamic pressure. The definition of force and moment coefficients is:

$$C_i = \frac{F_i}{\frac{1}{2}\rho_\infty V_\infty^2 S_{ref}} \quad i = A, N, Y \qquad (3)$$

$$C_{Mi} = \frac{M_i}{\frac{1}{2}\rho_\infty V_\infty^2 L_{ref} S_{ref}} \quad i = X, Y, Z \qquad (4)$$

with ρ_∞: atmospheric density, V_∞: speed relative to air.

$$L_{ref} = 0.16L \qquad (5)$$

$$S_{ref} = \frac{\pi L_{ref}^2}{4} \qquad (6)$$

However, please note that the present preliminary research effort investigated so far

longitudinal aerodynamic only, i.e. C_A, C_N and C_m. As mentioned above, aerodynamic coefficients are used at system level for the determination of launcher performances and control, as well as for general loading determinations. The launcher control always aims at a null global incidence of the vehicle, except during manoeuvres. Therefore, performances studies use only the axial force coefficient C_A as the aerodynamic force opposing to the movement. For the control software that commonly directs the thrust of nozzles in the proper direction, the main aerodynamic parameter is the evaluation of moment at the CoG location. Since propellants are constantly consumed along the flight, the CoG location is continuously changing too. Therefore, aerodynamic moments are provided at a conventional location, namely moment reference centre (MRC), see Fig. 2. For example, for ARIANE V this location is the main stage nozzle's gimbals point.

The flow regime, investigated for launcher aerodynamic appraisal, begins at null speed on the launch pad and goes up to hypersonic regime in high atmosphere, according to the flight domain in Fig. 3 [1].

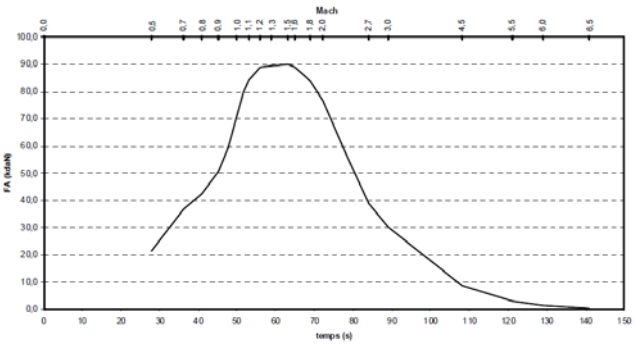

Fig. 3. The flight domain.

As shown, the main part of the needed characterizations is situated in the range $0.5 \leq M_\infty \leq 3$. Nevertheless, this remains a quite large domain to be covered, encompassing transonic-supersonic and hypersonic regimes [8]. Thus, in the light of the flight profile in Fig. 3, launcher aerodynamics has been addressed considering four Mach numbers, namely 0.5, 1.1, 2.5, and 5, at three angle of attacks, i.e., α=0, 5, and 7 deg, as summarized by the CFD test matrix in Tab. 1.

	Mach			
AoA, deg	0.5	1.1	2.5	5
0	E	E	E	E
5	E	E	E, NS	E, NS
7	E	E	E	E

E: Eulerian CFD
NS: Navier-Stockes CFD

Tab. 1. The CFD test matrix.

Therefore, Eulerian and Navier-Stokes 3-D CFD computations have been carried out on several unstructured hybrid meshes in motor-off conditions.

An overview of the mesh domain for both subsonic and sup-hypersonic speed flow is shown in Fig. 4. A blow-up of the mesh close and over the launcher is provided too.

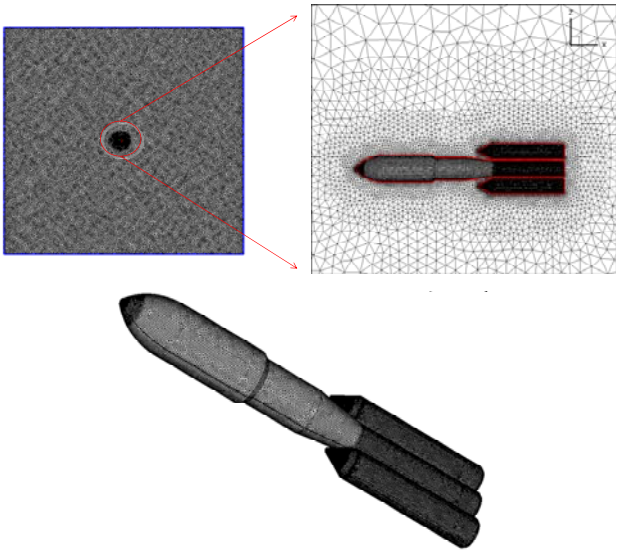

(a) Subsonic grid

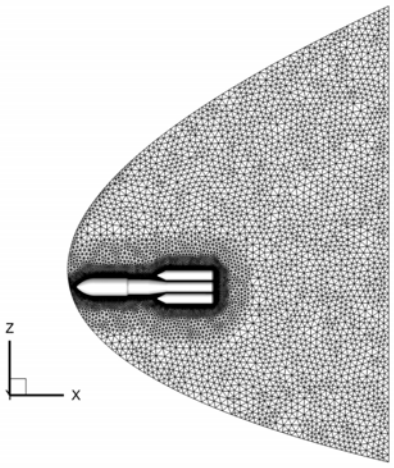

(b) Super-Hypersonic grid

Fig. 4. Overview of the hybrid mesh domain for both subsonic and sup-hypersonic speed.

As on can see, a square brick wide twenty body length upstream, downstream, upward and downward the launcher is considered to assure farfield unperturbed free-stream flow conditions at subsonic speed. Indeed, in this flow regime (i.e. elliptic flow), disturbances due to the body influence flow everywhere since they are propagated upstream via molecular collisions at approximately the speed of sound. Therefore, the computational domain must be wide enough to avoid interferences between flowfield and farfield boundary conditions.

On the other hand, at supersonic speed a shock wave appears at launcher leading edge (i.e., hyperbolic flowfield) because of, when flow moves faster than the speed of sound, disturbances cannot work their way upstream but coalesce forming a standing wave, namely bow shock. As a results, the computational domain is quite narrow, as shown in Fig. 4 (b).

CFD results of the preliminary assessment of launcher aerodynamics are summarized from Fig. 5 to Fig. 13 [8]. For instance, Fig. 5 shows the pressure distribution expected on the surface of the launcher flying at M_∞=0.5 and α=5 deg.

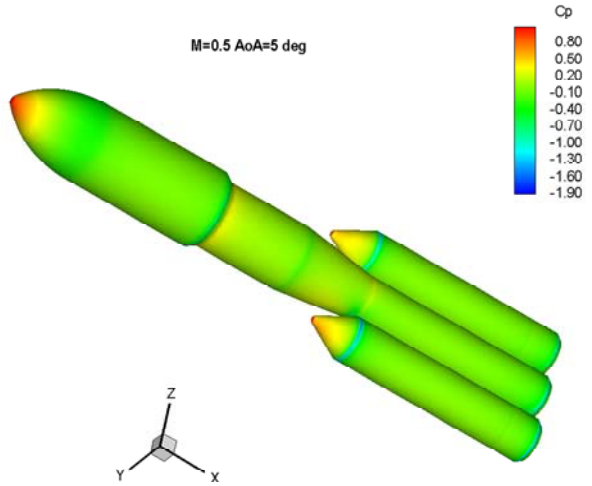

Fig. 5. Pressure coefficient at M_∞=0.5 and α=5 deg. Eulerian flow conditions (see Tab.1).

Flow compression that takes place for this flight conditions at the stagnation regions of launcher fairings and of booster conical forebodies is clearly shown. A recompression zone at the beginning of the cylindrical trunk, just after the fairings, and on that close to the booster forebodies can be noted as well [9].

Numerical investigations at higher Mach number are provided in Fig. 6. Here, an overview of pressure coefficient (C_p) distribution on launcher symmetry plane and surface evaluated at M_∞=2.5 and α=5 deg, is provided. Flow streamtraces on symmetry plane are reported as well.

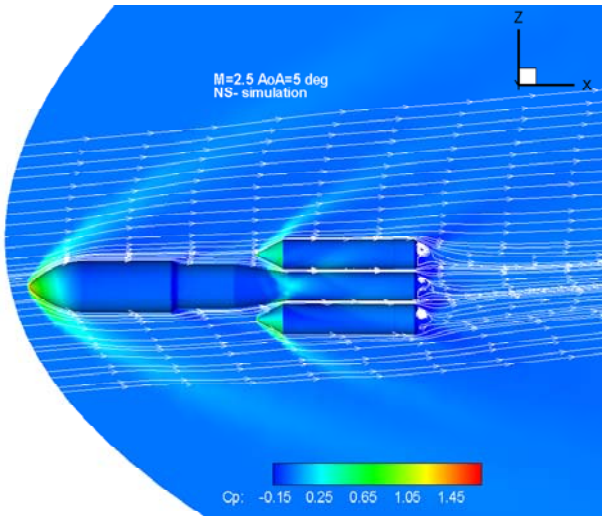

Fig. 6. Overview of C_p distribution on symmetry plane and launcher at M_∞=2.5 and α=5 deg.

The CFD computation is carried out with SST k-ω turbulence flow model and for cold wall boundary condition (i.e. T_w=300 K) [8], [9]. Results in Fig. 6 highlights a complex flowfield past the launcher due to the flow separation bubble at fairing boat-tail and the effect of fuselage/booster shock-shock interaction (SSI) and shock-wave boundary layer interaction (SWIBLI). For instance, after compression at conical flare of main fairings the flow undergoes to expansions that align it along with the constant cross section part of hammerhead. Hence, at the end of fairings another strong expansion takes place to accommodate the flow to the variation in launcher cross section (i.e., narrow cross section due to fairing boat-tail). Then, a shock wave arises at the beginning of the cylindrical trunk, just after the fairings, to redirect the flow along with the launcher wall [10].

Flow complexity increases further in the region close to the boosters leading edges, as shown in Fig. 7. In fact, in that region, complex SSI and SWIBLI phenomena take place. They result in higher thermo-mechanical loads (i.e. local pressure and thermal overshoots) on the launcher wall that must be carefully addressed in vehicle design [8], [9], [10].

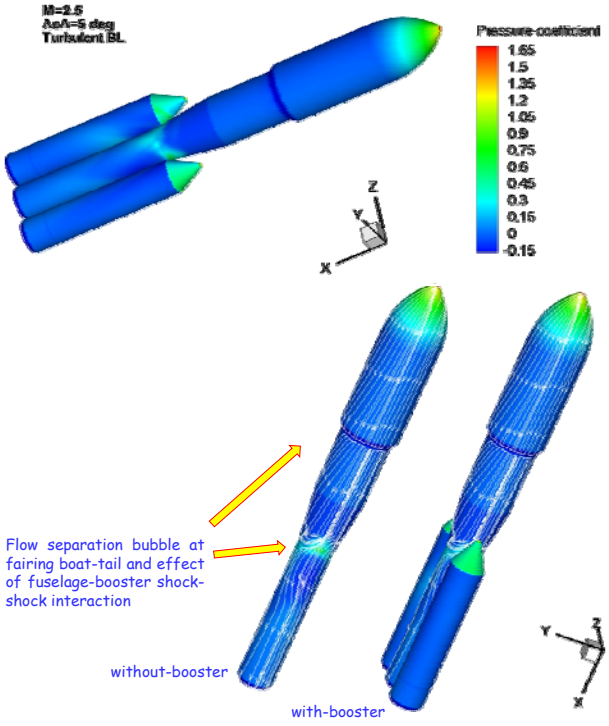

Fig. 7. Overview of C_p distribution on symmetry plane and launcher at M_∞=2.5 and α=5 deg.

The flowfield past the launcher at higher Mach number is shown in Fig. 8.

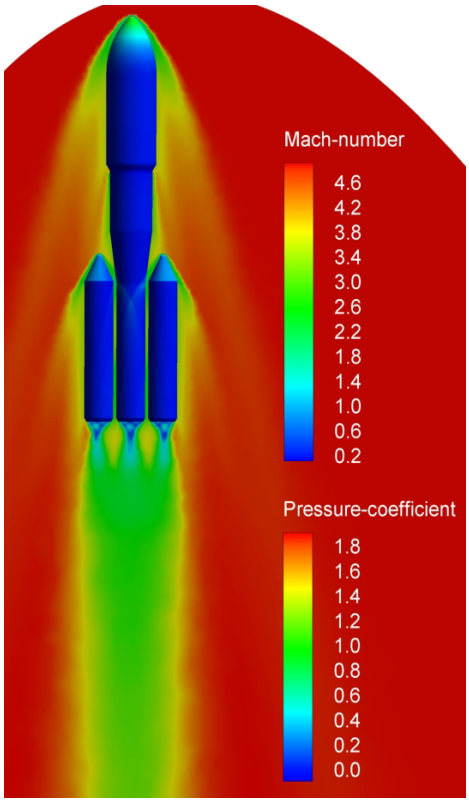

Fig. 8. Mach number field on symmetry plane and C_p on launcher surface at M_∞=5 and α=0 deg.

In this figure, the Mach number field on symmetry plane and pressure coefficient on launcher surface at M_∞=5 and α=0 deg are provided.

The effect of SSI between launcher and booster at these flight conditions are summarized in Fig. 9.

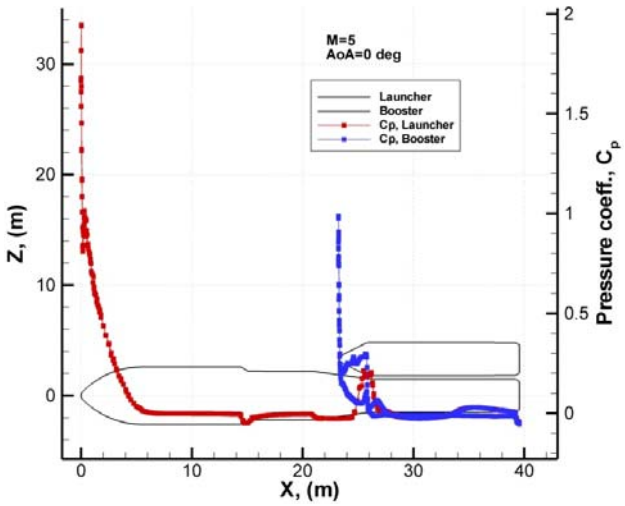

Fig. 9. Profiles of C_p on launcher and booster centerlines at M_∞=5 and α=0 deg.

As one can see, also at those flight conditions, complex flowfield interaction phenomena are expected.

As far as aerodynamic coefficients are concerned, launcher axial force, normal force and pitching moment coefficients versus Mach number are summarized from Fig. 10 to Fig. 12.

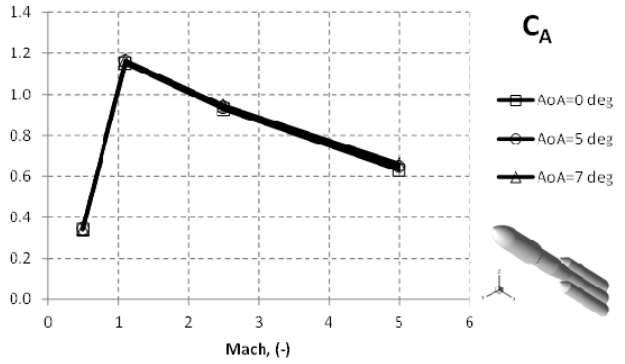

Fig. 10. Axial force coefficient versus Mach at different AoA, namely α=0, 5, and 7 deg.

Looking at the axial force coefficient, Fig. 10 points out that the C_A does not significantly change passing from 0 to 7 deg AoA at each considered Mach number.

On the contrary, the effect of flow compressibility is remarkable. Indeed, the strong increase to which undergoes the axial aerodynamic force, when M_∞ becomes transonic, is due to the wave drag contribution.

Nevertheless, this contribution tends to be less strong as Mach number goes towards hypersonic speed conditions considering that the shock becomes weak due to the streamlined vehicle aeroshape (i.e. high inclined shock to assure a narrow shock layer).

Regarding normal force coefficient numerical results in Fig. 11 highlight that, for each Mach number, C_N features a quite linear slope as α increases up to 7 deg AoA.

Also in this case, compressibility effect influences launcher normal force by means of different curve slopes for each Mach number case.

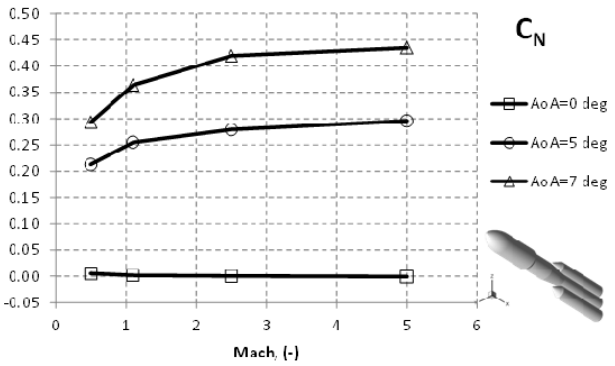

Fig. 11. Normal force coefficient versus Mach at different AoA, namely α=0, 5, and 7 deg.

Finally, the vehicle pitching moment coefficient features a behavior quite close to that described for the C_N with a strong pitch down detected for M_∞=5.

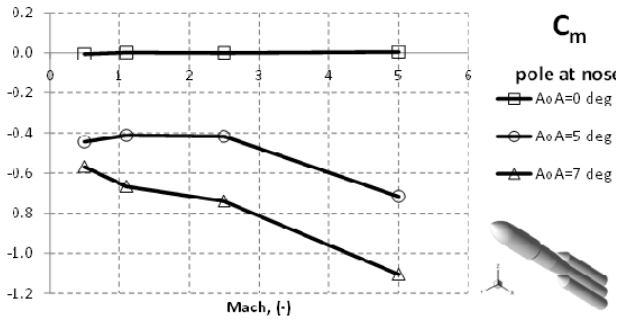

Fig. 12. Pitching moment coefficient versus Mach at different AoA, namely α=0, 5, and 7 deg.

Note that both C_N and C_m at α=0 deg are zero due to the symmetric launcher aeroshape.

Finally, axial coefficient breakdown is shown in Fig. 13.

As one can see, launcher fairings contribute to about 68% of total drag coefficient; while this percentage for booster fuselage and base is close to 21 and 5%, respectively.

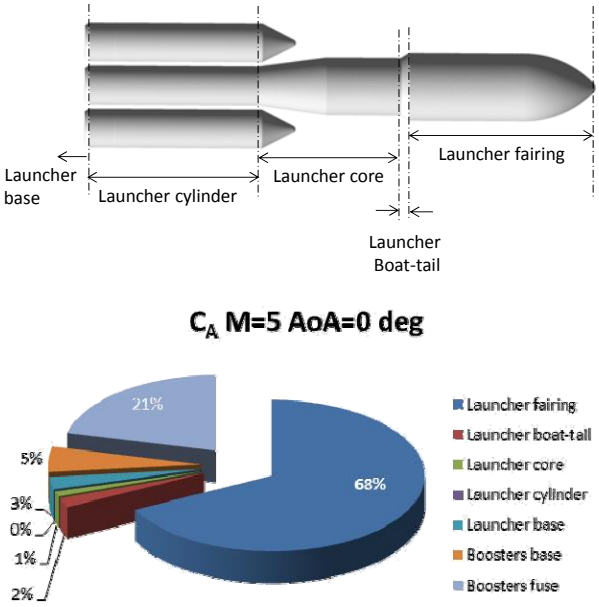

Fig. 13. C_A breakdown at M_∞=5 and α=0 deg.

4 Preliminary Assessment of Boosters Separation Dynamics

A critical point in the mission objective accomplishment is the safe separation dynamics of the boosters during flight [7],[11].

Keeping this in mind, a model for unsteady calculations has been set up to simulate the behaviour of the boosters dynamics while separating from launcher core at M_∞=5, α=0 deg and 0 deg of yaw angle.

These dynamic simulations are carried out by strongly coupling CFD flowfield analysis with a six degree-of-freedom (6 dof) solver for the booster dynamics. Indeed, at the time step (t_n), the unsteady CFD simulation provides the updated aerodynamic forces and moments acting on the booster [11].

Then, the six dof solver relocates the booster to a new position and orientation in the space in the following time step (t_{n+1}), by taking

into account for the body inertial and gravity field.

Hence, an updated mesh is built in the region between launcher and moving booster to allow CFD flowfield analysis past the moving body at the next time step [11].

Thus, in order to assess the dynamics of the booster relative to the core launcher, a dynamic meshing technique is exploited.

Finally, this process continues until last time step is reached, according to the flow chart in Fig. 14.

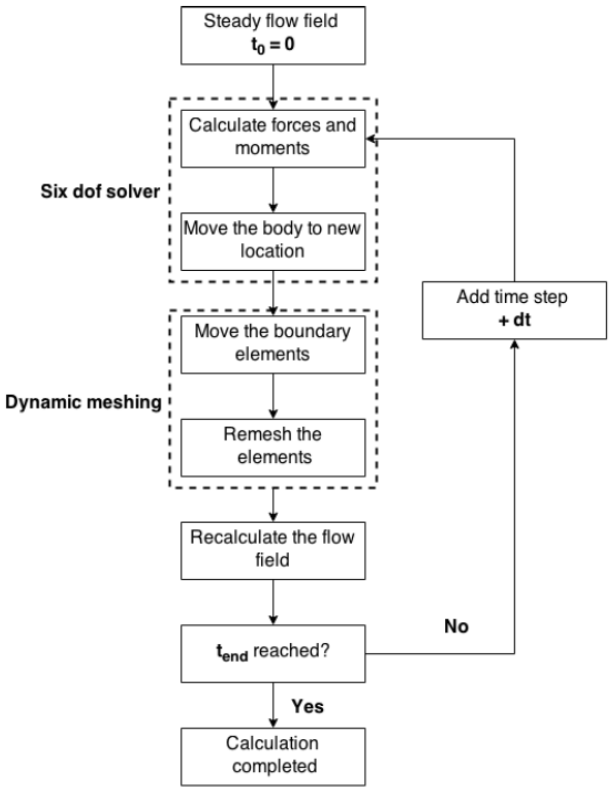

Fig. 14. Schematic overview of the separation analysis approach.

The translational movement of the booster CoG is computed with Fluent [12] in its own defined inertial coordinate system because this simplifies the equation to a form of $F = m \cdot a$

This equation applied to the body movement gives:

$$\dot{\vec{v}}_G = \frac{1}{m}\sum \vec{f}_G \qquad (7)$$

where $\dot{\vec{v}}_G$ is the acceleration for translational motion of the CoG and $\vec{f}_G$ are the aerodynamic and gravitational forces acting on the body and m is the mass of the rigid body.

Rotational motion is expressed in the body reference frame, so the angular movement is:

$$\dot{\vec{\omega}}_B = L^{-1}\left(\sum \vec{M}_B - \vec{\omega}_B \times L\vec{\omega}_B\right) \qquad (8)$$

where $\dot{\vec{\omega}}_B$ is the angular acceleration, L is the inertia tensor, $\vec{M}_B$ represents the moments acting on the body and $\vec{\omega}_B$ is the angular velocity.

Transformation between the inertia coordinate system and the body coordinate system can be carried out by multiplying with a transformation matrix, R

$$\vec{M}_B = R\vec{M}_G \qquad (9)$$

where R, reads:

$$R = \begin{bmatrix} \cos\theta\cos\psi & \cos\theta\sin\psi & -\sin\theta \\ \sin\phi\sin\theta\cos\psi - \cos\phi\sin\psi & \sin\phi\sin\theta\sin\psi + \cos\phi\cos\psi & \sin\phi\cos\theta \\ \cos\phi\sin\theta\cos\psi + \sin\theta\sin\psi & \cos\phi\sin\theta\sin\psi - \sin\phi\cos\psi & \cos\phi\cos\theta \end{bmatrix}$$

and ϕ, θ, and ψ are respectively the rotations about the x-, y-, and z-axis.

Once the angular and the translational accelerations are computed from Equation (7) and Equation (8), the rates are derived by numerical integration. The angular and translational velocities are used in the dynamic mesh calculations to update the rigid body position.

Preliminary results of this numerical investigation are provided in Fig. 15 at several time steps, namely t_0, t_1, t_2, t_3, t_4, and t_5 (t_0=0 s is the separation instant).

From Fig. 15 it can be appreciated how the booster's centre of gravity (CoG) moves downstream of the launcher.

In particular, the trajectory (relative to launcher core) of the booster CoG in the launcher symmetry plane (x-z plane) and the rotation about booster y-axis can be inferred from Fig. 15.

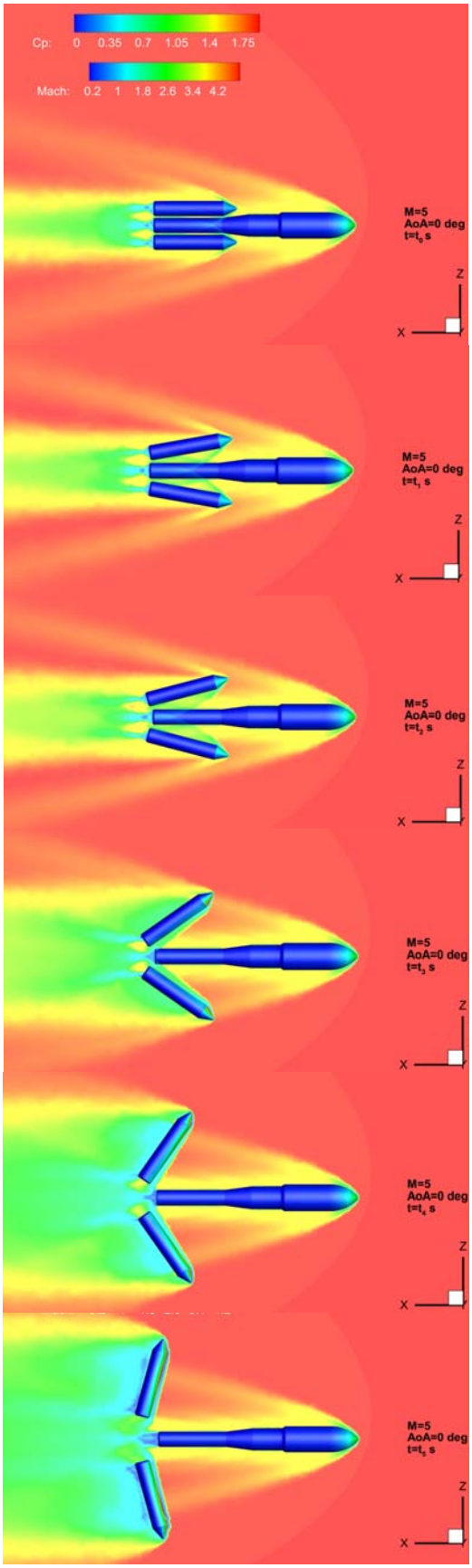

Fig. 15. Detailed view of separation dynamics at different time steps at M_∞=5, α=0 deg.

5 Conclusions

In this research effort launcher aerodynamic design activities at phase-A level are described.

The goal is to address the preliminary aerodynamic database of a next generation launch vehicle as input for performances evaluations as well as launcher control, sizing, and staging dynamics. To this end, steady state computational fluid dynamics, with both Euler and Navier-Stokes approximations, are carried out at four Mach numbers, namely 0.5, 1.1, 2.5, and 5, and at three angle of attacks, i.e., α=0, 5, and 7 deg,. For this test matrix launcher aerodynamic performance in terms of axial, normal and pitching moment coefficients is provided. Numerical results point out that the axial force coefficient does not significantly change passing from 0 to 7 deg angle of attack at each considered Mach number; while the effect of flow compressibility is remarkable.

Regarding normal force coefficient results highlight that, for each Mach number, it features a quite linear slope as the angle of attack increases up to 7 deg. Finally, the vehicle pitching moment coefficient features behaviour quite close to that described for the normal force coefficient, but a strong pitch down is detected for Mach 5.

Finally, preliminary results about boosters separation dynamics are also provided by means of a fully coupled approach between unsteady computational fluid dynamics and 6 degree-of-freedom trajectory analysis.

Preliminary numerical results figure out that the booster does not collide at passive staging conditions, when the launcher is flying at 0 deg angle of attack and Mach 5.

6 References

[1] J.F., Pallegoix, *Launcher aerodynamics*. STO-EN-AVT-206. 2014.

[2] A., Viviani, and G., Pezzella, *Aerodynamic and Aerothermodynamic Analysis of Space Mission Vehicles*. Springer International Publishing. DOI: 10.1007/978-3-319-13927-2. Hardcover ISBN 978-3-319-13926-5. eBook ISBN: 978-3-319-13927-2.

[3] A., Viviani, and G., Pezzella, *Next Generation Launchers Aerodynamics*. Research Signpost, T.C. 37/661 (2), Fort P.O., Trivandrum-695 023. Kerala, India. ISBN: 978-81-308-0512-2.

[4] P. Catalano, M. Marini, A. Nicolì, and A. Pizzicaroli. "CFD Contribution to the Aerodynamic Data Set of

the Vega Launcher", *Journal of Spacecraft and Rockets*, Vol. 44, No. 1 (2007), pp. 42-51. http://dx.doi.org/10.2514/1.23534

[5] J., J. Bertin, "Hypersonic Aerothermodynamics". AIAA Education Series. 1994.

[6] J. D., Anderson, "Hypersonic and High Temperature Gas Dynamics", McGraw-Hill Book Company, New York, 1989.

[7] M. Genito, F. Paglia, A. Mogavero, D. Barbagallo, "1st Stage Separation Aerodynamics of Vega Launcher". 7th European Symposium on Aerothermodynamics. Brugge, Belgium. 9-12 May 2011. ESA SP-692.

[8] A., Viviani, G., Pezzella, "Computational Flowfield Analysis of a Next Generation Launcher". 6th European Conference for Aeronautics and Space Sciences (Eucass). 29 June- 3 July. 2015 Krakow. Poland.

[9] A., Viviani, G., Pezzella, "Numerical Analysis of the Flowfield Past a Next Generation Launcher". 20th AIAA Hypersonics. Strathclyde University Technology & Innovation Center. 6-9 July 2015 Glasgow. Scotland. AIAA-2015-3535. doi: 10.2514/6.2015-3644.

[10] G. Pezzella, M. Marini, P. Roncioni, J. Kauffmann, C. Tomatis. "Preliminary Design of Vertical Takeoff Hopper Concept of Future Launchers Preparatory Program". Journal of Spacecraft and Rockets 2009. ISSN 0022-4650 vol.46 no.4 (788-799) doi: 10.2514/1.39193.

[11] G. Pezzella, S. van Brummen, J. Steelant, "Assessment of Hypersonic Aerodynamic Performance of the EFTV-ESM Configuration in the Framework of the Hexafly-Int Research Project", 8th European Symposium on Aerothermodynamics for Space Vehicles. 2-6 March 2015. Lisbon. Portugal. European Space Agency.

[12] ANSYS, Inc. ANSYS Fluent Theory Guide, 2013.

7 Contact Author Email Address

Authors email address are:
antonio.viviani@unina2.it
g.pezzella@cira.it
egidio.d'amato@gmail.com

Copyright Statement